Relaxation of the first excited 1_u state of Hg$_2$

M. Stock,[a] E. W. Smith, R. E. Drullinger, and M. M. Hessel

Laser Physics Section, National Bureau of Standards, Boulder, Colorado 80302
(Received 3 November 1977)

The decay of the 335 nm Hg$_2$ fluorescence band was measured with 1 nsec time resolution for the first 200 nsec following optical excitation by a 10 nsec laser pulse. Measurements of the decay rates for various wavelengths in this band were used to analyze the relaxation of the vibrational levels in the 1_u state. It was found that the lower vibrational levels quickly reach a Boltzmann distribution described by an effective temperature T_{eff}. This effective temperature then decreases with time, asymptotically approaching the gas temperature. Comparison of these data with a model calculation by Montroll and Shuler yields a transition rate of 5.2×10^{-11} cm^3 sec^{-1} for the transition between the two lowest vibrational states. Analysis of the relaxation for higher vibrational levels gave a value of 2.7×10^{-10} cm^3 sec^{-1} for the $1_u \rightarrow 0_g^-$ transition rate. Since no mercury trimers have been formed at these early times, the 485 nm fluorescence band is not present. It was therefore possible to evaluate the repulsive wall of the 1_u potential curve for small internuclear distances corresponding to wavelengths in the red wing of the 335 nm dimer band which are normally overlapped by the 485 nm trimer band.

I. INTRODUCTION

In a previous paper,[1] the relaxation of optically excited mercury vapor was analyzed in terms of a simple kinetic model. It had been shown[2,3] that the 335 nm fluorescence band arises from the first excited 1_u state of Hg$_2$ and the 485 nm fluorescence band arises from an excited mercury trimer state[1] which lies 6500 cm^{-1} below the 1_u dimer state. The presence of low lying metastable dimer states had been predicted theoretically,[4,5] and in Ref. 1 it was shown that the lowest of these lies about 2800 cm^{-1} below the 1_u state (see Table I of Ref. 1) The analysis in Ref. 1 was based on the decay of the molecular fluorescence bands at late times (1–2000 μsec) following the 10 nsec exciting laser pulse. For these times, both bands decay exponentially with the same decay constant. It was argued that the energy reservoirs at these late times were the $6\,^3P_0$ atomic state (optically excited by the pump laser) and the low lying metastable (gerade) dimer states (populated mainly by three body recombination of $6\,^3P_0 + 6\,^1S_0$ atoms); there was no indication of any trimer metastable levels below the state radiating the 485 nm band.

In the present paper we will study the decay of the molecular fluorescence at several different wavelengths within the 335 nm band during the first 200 nsec following the exciting laser pulse. The apparatus is identical to that used in Ref. 1 except that the transient digitizer was replaced by a unit having 1 nsec time resolution. Briefly, this apparatus employed a frequency-doubled dye laser pumped by a nitrogen laser. For the measurements reported in this paper, the doubling crystal was tuned to 254.5 nm (see Fig. 1.) The 10 nsec, 15 kW laser pulse at 254.5 nm was used to excite the mercury vapor in a two compartment cell in which vapor temperature and density could be controlled independently. The molecular fluorescence was scanned with

a 0.1 m monochromator (2.0 nm resolution) coupled to a transient digitizer (1 nsec time resolution) and a minicomputer which averaged subsequent shots and stored the data on magnetic tape for later analysis.

The difference between the analysis of Ref. 1 and the present paper is illustrated in Fig. 2 which is a plot of the fluorescence intensity at 340 nm as a function of time. This wavelength is emitted primarily by the lowest vibrational levels of the 1_u state (see Table II of Ref. 3). The plot shows a sharp intensity spike within the first 50 nsec followed by a slow rise and decay between 0.5 μsec and 200 μsec. The decay of the slower feature (10–200 μsec) was analyzed in Ref. 1 and in the present paper we will study the decay of the intensity spike at early times (20–50 nsec in this plot).
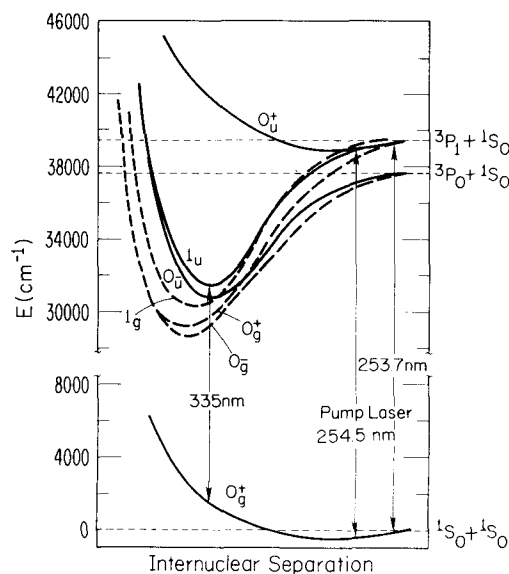

FIG. 1. Theoretical estimates[5] of several low lying Hg$_2$ potential curves based on *ab initio* calculations for Mg$_2$ and experimental observations of Hg$_2$. The pump laser transition is shown as well as the center of the 355 nm fluorescence band.

[a] Postdoctoral Research Fellow supported by the Deutsche Forschungs Gemeinschaft. Present address: Universität Kaiserslautern, Fachbereich Physik, 675 Kaiserslautern, Germany.
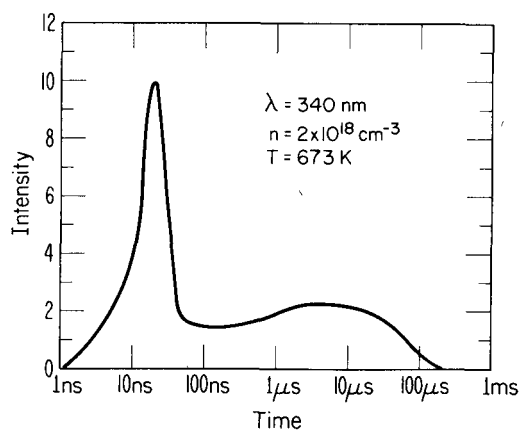
FIG. 2. Typical plot of intensity vs time (on a log scale) for a wavelength in the 355 nm band. The decay of the intensity spike at early times (10–100 nsec) is the feature studied in the present paper. The peak of the intensity spike follows the peak of the pump laser pulse by about 1 or 2 nsec, but it is difficult to compare the two since the laser pulse is about 10^6 times more intense.

The intensity spike of interest represents a very small fraction of the total fluorescence intensity emitted at any given wavelength (about 0.5% in Fig. 1) hence we are always faced with weak signals and must average over several shots. Nonetheless, this spike is always readily distinguishable from the rise of the slower component.

The physical processes involved in our optical pumping scheme (discussed in Sec. II of Ref. 1) may be used to give a physical interpretation of the features in Fig. 2. The 254.5 nm pump laser populates highly excited vibrational levels of the 1_u state (e.g., Fig. 1). This excitation may be vibrationally stabilized directly to lower vibrational levels or converted into $6\,^3P_0$ and $6\,^3P_1$ atoms by dissociation of the excited 1_u molecules. The $6\,^3P_0$ atoms act as a metastable energy reservoir which feeds excitation to the molecular states via three-body recombination with ground state atoms. We have measured the rise times of the slow feature in Fig. 2 and find that they coincide with the known[1,6] decay times for $6\,^3P_0$ atoms. The rise of the slow component is therefore due to the $6\,^3P_0$ atoms slowly feeding excitation back to the molecular states. This excitation is then collisionally distributed among the various molecular levels and finally decays away due to emission in the 335 nm and 485 nm fluorescence bands. The rise of the initial intensity spike immediately follows the pump laser pulse (lagging by 0–10 nsec depending on gas density and fluorescence wavelength) and its decay is proportional to the gas density for $n \geq 5 \times 10^{17}$ cm^{-3}. This spike is therefore interpreted as resulting from binary collision relaxation of the vibrational levels which transfers excitation from the states directly excited by the pump laser to lower levels. By studying the temperature and density dependence of this decay, we can then obtain information as to the relaxation processes involved and their rate coefficients. This will be discussed in Sec. III.

At the early times when the intensity spike is present, there is no measurable emission in the 485 nm band. This is due to the fact that the 485 nm band is emitted by Hg_3 which is formed via three-body recombination of Hg_2 with ground state mercury atoms. This three-body process proceeds at roughly the same rate as the rise of the slow component, hence the intensity of the 485 nm band roughly coincides with the slow feature in Fig. 2 (the two are of course not identical, as can be seen in Figs. 3–5 of Ref. 1).

The absence of trimer emission at early times permits an analysis of the red wing of the 335 nm band which would normally be masked by overlap with the blue wing of the 485 nm band.[2] We are therefore able to evaluate the repulsive wall of the 1_u potential energy curve for small internuclear separations as discussed in Sec. IV.

II. POPULATION DISTRIBUTION

The number of photons emitted at wavelength λ can be written in the form [e.g., Eq. (2.1) of Ref. 3]

$$I_\lambda \, d\lambda = \frac{A(\lambda)\phi(\lambda)}{\lambda^2} \, n_\lambda \, d\lambda \,, \tag{2.1}$$

where $A(\lambda)$ and $\phi(\lambda)$ denote the A value and line profile, and n_λ denotes the number of states which can emit the wavelength λ.

In general, n_λ is expressed as a sum over a set of vibration–rotation states weighted by their populations and probabilities of emission. For heavy molecules such as Hg_2, the separation of the rotational energy levels is so small that the individual rotational lines are spectroscopically unresolved. The experimentally determined values of n_λ are therefore effectively averaged over rotation hence n_λ may be regarded as the population of the vibrational level which gives rise to emission at the wavelength λ. At our temperatures, $T > 473\,°K$, the width of most vibrational lines is greater than their separation; hence they too are spectroscopically unresolved. Furthermore, our 2 nm spectroscopic resolution corresponds to about 150 cm^{-1}, which is roughly one vibrational spacing.[2,3,7] Thus our n_λ actually contains contributions from two or three vibrational states lying close to the vibrational energy level E_λ which dominates the emission at wavelength λ.

Using the known values of $A(\lambda)\phi(\lambda)$ (from Table II of Ref. 3) and the measured values of I_λ, Eq. (2.1) enables us to plot n_λ as a function of time for several different wavelengths λ in the 340 nm band. Figure 3 shows typical results at a temperature of 673 °K and a gas density of 5×10^{17} cm^{-3}. The time $t = 0$ was chosen to lie about 5 nsec before the peak of the pump laser pulse (the latter has a half-width of 10 nsec).

The population density at each wavelength rises then decays exponentially with time. These exponential decay rates were measured for several different densities for a fixed temperature of 673 °K (Fig. 4) and for several temperatures at a fixed density of 2×10^{17} cm^{-3} (Fig. 5). Measurements of the exponential decay co-
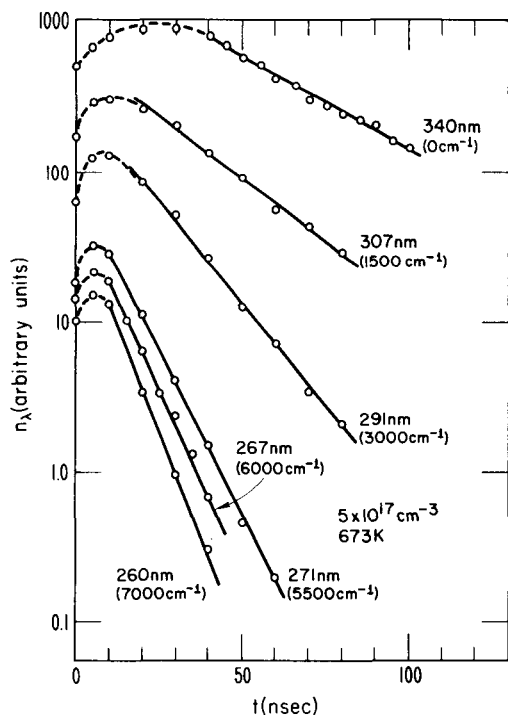
FIG. 3. Populations n_λ vs time for various wavelengths in the 355 nm band. Numbers in parenthesis give the vibrational energy of the level which dominates the emission at each wavelength plotted. The time $t = 0$ lies about 5 nsec before the peak of the pump laser pulse which has a width of about 10 nsec. The solid lines denote the region of exponential decay.

efficient were limited to gas densities of 10^{17} cm⁻³ or higher due to the weak fluorescence intensity at low densities. At high densities (above 10^{18} cm⁻³), the three-body molecular formation rate from the $6\,^3P_0$ atomic state becomes appreciable and tends to obscure the exponential decay measurements.
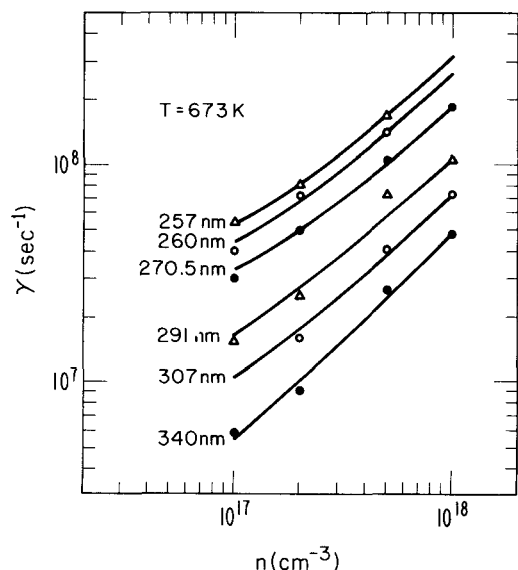

FIG. 4. Decay coefficient vs density for several wavelengths at a temperature of 673 °K. The solid curves are a least squares fit to the data using the function $\gamma_\lambda = \tau_\lambda^{-1} + nk_\lambda$.
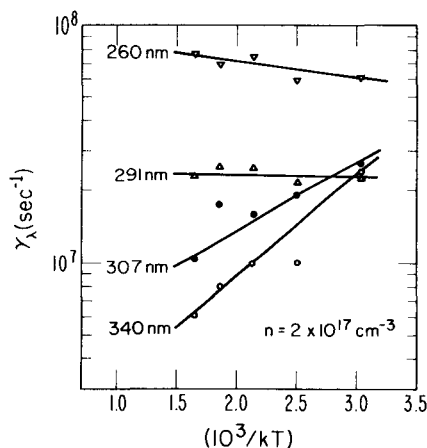

FIG. 5. Temperaure dependence of the decay coefficients at several wavelengths for a density of 2×10^{17} cm⁻³. kT is in cm⁻¹.

Before analyzing the decay coefficients, it is interesting to plot the population densities n_λ as a function of the vibrational energy E_λ of the state which emits at the wavelength λ. These vibrational energies, as determined from Table II of Ref. 3, were also used to label the curves in Fig. 3. In Fig. 6, n_λ is plotted as a function of E_λ at several different times. The solid lines represent a fit to the data using a Boltzmann distribution function $n_\lambda(t) = n_{340}(t) \exp[-E_\lambda/kT_{eff}(t)]$, where $n_{340}(t)$ is independent of E_λ, and $T_{eff}(t)$ is a time dependent effective vibrational temperature (recall that the emission at $\lambda = 340$ nm results from vibrational states at the bottom of the 1_u well, hence $E_{340} = 0$). At the very early times, the populations of the higher levels, $E_\lambda \gtrsim 5500$ cm⁻¹, lie above this Boltzmann distribution but, due to their rapid decay rates, they quickly come into equilibrium at the vibrational temperature $T_{eff}(t)$. For 20 nsec $\leq t \leq 60$ nsec, all the levels are well described by the Boltzmann distribution. At late times, $t > 60$ nsec in Fig. 6, the higher levels, $E_\lambda \geq 550$ cm⁻¹, fall below the Boltzmann population, again due to their more rapid decay rates. Similar plots have been made for densities ranging from 10^{17} cm⁻³ to 2×10^{18} cm⁻³ and gas temperatures from 450 °K to 1073 °K and the same general behavior was observed in all cases, namely, the population can be well approximated by a Boltzmann distribution with a time dependent effective temperature $T_{eff}(t)$ during most of the times of interest. The higher levels, $E_\lambda \gtrsim 5500$ cm⁻¹, tend to lie above the Boltzmann population at very early times and they fall below at very late times.

The effective vibrational temperature $T_{eff}(t)$ is plotted as a function of time in Fig. 7. In general, this vibrational temperature decreases asymptotically to the gas temperature. In fact, for $n = 10^{17}$ cm⁻³ and $T = 1073$ °K, T_{eff} became equal to the gas temperature at 275 nsec and remained at that value for over 100 nsec until the signal was overwhelmed by the leading edge of the slow intensity component (see Fig. 2). It is interesting to note that the vibrational temperature at early times is decreased by raising the gas tem-

perature; this trend must of course be reversed at late times because T_{eff} asymptotically approaches the gas temperature. This result simply means that the vibrational population is always much closer to thermal equilibrium at the gas temperature when the latter is increased. Figure 7 also shows that T_{eff} decreases much more rapidly at higher densities; this is not at all surprising since the vibrational relaxation rates are essentially proportional to n (see Fig. 4).

III. ANALYSIS OF DECAY COEFFICIENTS

In order to analyze the measurements of the decay coefficient, we first note that the population density of the vibrational level E_λ will in general be described by a kinetic equation of the form

$$\dot{n}_\lambda(t) = \tau_\lambda^{-1} n_\lambda(t) - \int [R(E_\lambda', E_\lambda) + r(E_\lambda', E_\lambda)] n_\lambda(t) \, dE_\lambda$$

$$+ \int [R(E_\lambda, E_\lambda') n_\lambda'(t) + r(E_\lambda, E_\lambda') m_\lambda'(t)] dE_\lambda' .$$

(3.1)

In the first term, τ_λ represents the collisionless (e.g., radiative, etc.) lifetime of the vibrational state which is responsible for emission at the wavelength λ. Since vibrational levels lying above the $6\,^3P_0$ atomic state can spontaneously dissociate to $6\,^3P_0 + 6\,^1S_0$ atoms via rotational mixing of the 1_u and 0_u^- states at small internuclear distances (see Fig. 1), τ_λ must also include the effect of this collisionless dissociation for these high lying vibrational levels. The second term represents collisional losses due to transitions from the level E_λ to other levels E_λ' including pure vibrational transitions within the 1_u state denoted by $R(E_\lambda', E)$ as well as transitions to other electronic states denoted by $r(E_\lambda', E_\lambda)$. The third term is the rate at which collisions transfer population into the level E_λ from other vibrational levels within the 1_u state, $R(E_\lambda, E_\lambda') n_\lambda'(t)$, and from other electronic states, $r(E_\lambda, E_\lambda') m_\lambda'(t)$, where $m_\lambda'(t)$ denotes the population of the level E_λ' in electronic states other than 1_u. Since we are only interested in describing n_λ during the time when it is decaying exponentially, we will look for solutions $n_\lambda(t)$ of the form $\exp(-\gamma_\lambda t)$. Equation (3.1) then gives

$$\gamma_\lambda = \tau_\lambda^{-1} + \int [R(E_\lambda', E_\lambda) + r(E_\lambda', E_\lambda)] dE_\lambda' - \int [R(E_\lambda, E_\lambda') \{n_\lambda'(t)/n_\lambda(t)\} + r(E_\lambda, E_\lambda') \{m_\lambda'(t)/n_\lambda(t)\}] dE_\lambda' = \tau_\lambda^{-1} + nk_\lambda ,$$

(3.2)

where the collisional gain and loss terms have been combined to give a net collisional relaxation rate nk_λ (n being the gas density). It should be noted that the collisional gain term contains the population ratios $n_\lambda'(t)/n_\lambda(t)$ and $m_\lambda'(t)/n_\lambda(t)$, which are in general time de-

pendent. However, during the times of interest to us (i.e., the time interval when n_λ is decaying) the integrand of this gain term is sharply peaked about $E_\lambda' = E_\lambda$ where the population ratios are not time dependent. To show this, we first note that when $E_\lambda' > E_\lambda$ the population ratios are proportional to $\exp[-(E_\lambda' - E_\lambda)/kT_{eff}(t)]$, where T_{eff} is the vibrational temperature discussed in the previous section. When $E_\lambda' < E_\lambda$, the transition rates R and r are proportional to $\exp[-(E_\lambda - E_\lambda')/kT]$ since this case corresponds to transitions upward in energy; the integrand is thus proportional to $\exp[-(E_\lambda - E_\lambda')(1/kT - 1/kT_{eff})]$. Since $T_{eff} > T$ when the system is decaying, we see that the integrand of the gain term is exponentially peaked about the point $E_\lambda = E_\lambda'$, where its time dependence vanishes. Furthermore, when n_λ is decaying,
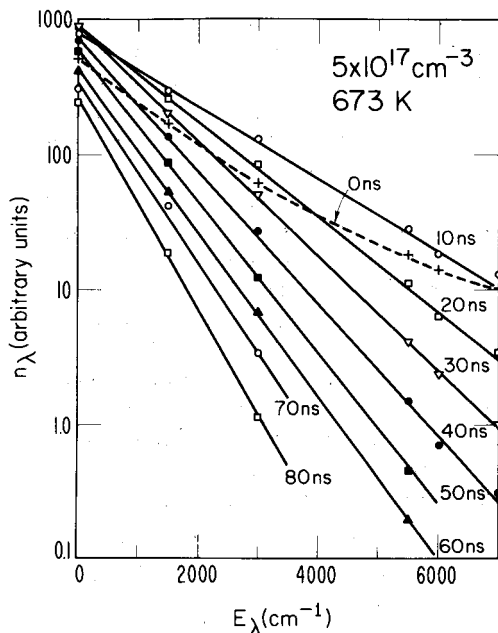

FIG. 6. Populations n_λ vs vibrational energy E_λ at several times following the exciting laser pulse. The time $t = 0$ lies about 5 nsec before the peak of the pump laser pulse which has a width of about 10 nsec. The solid lines denote a fit to the data using a Boltzmann distribution function with a time dependent effective vibrational temperature, T_{eff} (t). The latter is plotted in Fig. 7.
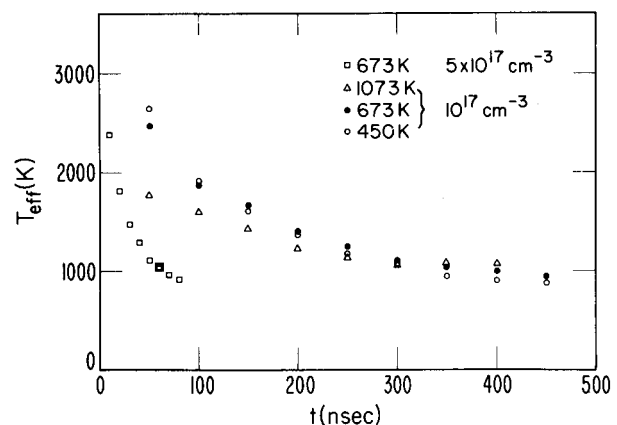

FIG. 7. Effective vibrational temperature as a function of time for various gas temperatures and densities. In all cases T_{eff} (t) asymptotically approaches the gas temperature at late times.

the loss term is greater than the gain term, thus further reducing the effect of any time dependence in k_λ. It is therefore not surprising to find a region of time where k_λ and thus γ_λ are independent of time and $n_\lambda(t) \propto \exp(-\gamma_\lambda t)$. It must be emphasized that Eq. (3.2) is valid only over the time interval when $n_\lambda(t) \propto \exp(-\gamma_\lambda t)$. This is not the case at late times when $T_{eff}(t)$ approaches the gas temperature T because the factor $\exp\{-(E_\lambda - E'_\lambda)[1/kT - 1/kT_{eff}(t)]\}$ in the gain term approaches unity, the contribution from $E'_\lambda < E_\lambda$ increases, and the time dependence of the factor $n'_\lambda(t)/n_\lambda(t)$ becomes appreciable. In fact, when $T_{eff}(t) = T$, the gain term just cancels the loss term hence $\gamma_\lambda \rightarrow \tau_\lambda^{-1}$ at late times. It was not possible to make definitive measurements of this process because three body molecular formation from the $6\,^3P_0$ atomic state also becomes important at late times.

A least squares fit was used to determine the values of τ_λ^{-1} and k_λ from the experimental data. Our values of τ_λ^{-1} are plotted in Fig. 8 as a function of vibrational energy E_λ and a comparison is made with radiative lifetimes calculated from the A values in Table II of Ref. 3. The latter values for τ_λ^{-1} were obtained by adding the A values[8] for the two radiative transitions out of each vibrational level. For example, $\tau^{-1} = A_{305} + A_{370} \simeq 4.3 \times 10^6 \times \text{sec}^{-1}$ for the vibrational level lying 1660 cm^{-1} above the bottom of the 1_u well since this level emits at both 305 and 370 nm (see Table II of Ref. 3). Unfortunately, the A values for $\lambda > 370$ nm (corresponding to $E_\lambda > 1680$ cm^{-1})

are unknown and were therefore not included for states above 1680 cm^{-1}. The contribution from these A values is probably negligible in any case because the A values drop off rather rapidly in the red wing of the band whereas they become quite large in the blue wing. That is, the radiative lifetime of the higher vibrational levels is determined primarily by radiative transitions in the blue wing for which the A values are known.

The agreement between our measured lifetimes and the purely radiative lifetimes calculated from Ref. 3 is excellent for the lower levels $E_\lambda < 3000$ cm^{-1}. For $E_\lambda > 3000$ cm^{-1}, the values of τ^{-1} obtained from Ref. 3 decrease whereas the values obtained in the present work continue to increase with the largest value $\tau_{257}^{-1} = 2.4 \times 10^7$ sec^{-1} being more than twice as large as the radiative A value for the 253.7 nm atomic line.[9] The fact that some of our values for τ^{-1} exceed $A_{253.7}$ is not surprising because our measured lifetimes include the effect of collisionless dissociation which will decrease the lifetimes for vibrational levels lying above the $6\,^3P_0$ atomic state (i.e., $E_\lambda \gtrsim 6000$ cm^{-1}). This cannot explain the discrepancy with the values obtained from Ref. 3 for $E_\lambda \simeq 3125$ cm^{-1} and 3600 cm^{-1} because collisionless dissociation should not be important for such low vibrational levels. We therefore suspect that the A values in Ref. 3 are in error for $\lambda \gtrsim 290$ nm; this seems plausible because the method of analysis used in Ref. 3 is subject to its greatest error near the band edges and the A values are particularly sensitive, as noted on p. 5674 of Ref. 3.

We note finally that the values of τ_λ^{-1} increase *linearly* with the vibrational energy for $E_\lambda \gtrsim 1000$ cm^{-1}. The reason for this linear increase is not known but its consequences are discussed below.

The values of the collisional relaxation rate k_λ are plotted in Fig. 9 as a function of vibrational energy E_λ and it is noted that k_λ may be approximated by the function $k_\lambda = 4.7 \times 10^{-11} \exp(E_\lambda/4240)$, where E_λ is in cm^{-1} and k_λ is in cm^3 sec^{-1}. This function is essentially linear in E_λ for $E_\lambda \lesssim 4000$ cm^{-1} and, since τ_λ^{-1} is also linear in E_λ, we may write

$$\gamma_\lambda = \tau_\lambda^{-1} + nk_\lambda \simeq \gamma_{340} + \beta E_\lambda \quad (E_\lambda \lesssim 4000 \text{ cm}^{-1}), \qquad (3.3)$$

where β is a constant that depends on the gas density and temperature. If we now choose the earliest time t_0 at which n_λ is described by a Boltzmann distribution, then

$$n_\lambda(t) = n_\lambda(t_0)\, e^{-\gamma_\lambda(t-t_0)}$$
$$= n_\lambda(t_0)e^{-\gamma_{340}(t-t_0)}\, e^{-\beta E_\lambda(t-t_0)}$$
$$= n_{340}(t)[n_\lambda(t_0)/n_{340}(t_0)]\, e^{-\beta E_\lambda(t-t_0)} \qquad (3.4)$$
$$= n_{340}(t)e^{-E_\lambda/kT_{eff}} ,$$

where

$$\frac{1}{kT_{eff}(t)} \equiv \frac{1}{kT_{eff}(t_0)} + \beta(t-t_0) . \qquad (3.5)$$

This explains the observation in the previous section that once the lower vibrational levels ($E_\lambda \lesssim 4000$ cm^{-1}) reach a Boltzmann distribution, they remain in a Boltzmann distribution as the states decay and the effective
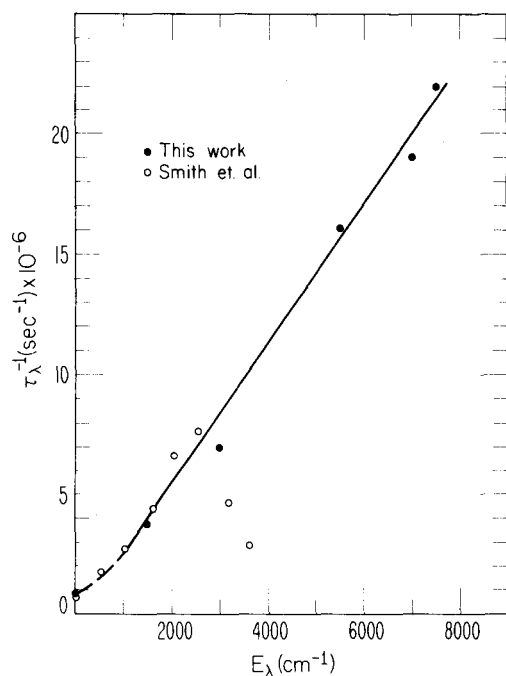

FIG. 8. The values of τ_λ^{-1} obtained in this work (solid data points) are compared with radiative decay rates obtained from Table II of Ref. 3 (open circles) as a function of vibrational energy E_λ. The curve drawn through the points is a rough fit to the data; the solid portion is proportional to E_λ and is intended to show that τ_λ^{-1} essentially linear in E_λ. Disagreement with data from Ref. 3 around 3000 cm^{-1} is tentatively ascribed to inaccuracy in the method of analysis used in Ref. 3 for data near the edge of the fluorescence band.
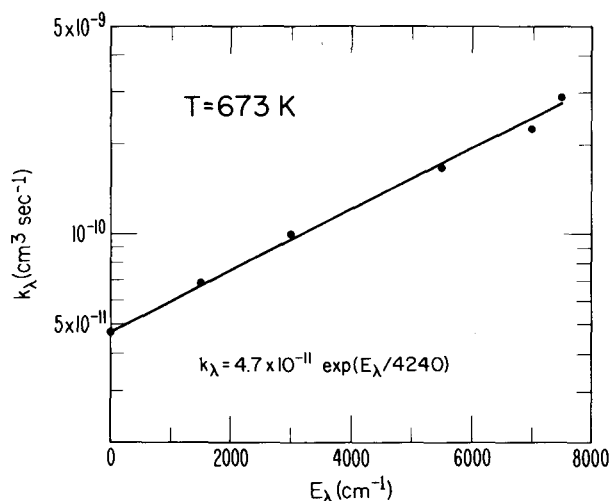
FIG. 9. Collisional decay coefficient k_λ as a function of vibrational energy for a gas temperature of 673 °K. The solid curve shows that the data may be approximated by $k_\lambda = 4.7 \times 10^{-11} \exp (E_\lambda/4240)$, where E_λ is in cm^{-1} and k_λ is in cm^3 sec^{-1}.

temperature decreases. This behavior is a consequence of the fact that γ_λ is linear in E_λ for $E_\lambda \lesssim 4000 \ cm^{-1}$. For the higher levels, $E_\lambda > 4000 \ cm^{-1}$, the values of k_λ are larger than the linear approximation hence the decay rate γ_λ will be too large for these states to remain in a Boltzmann distribution. This explains the observation that the populations of the high lying levels start out above the Boltzmann distribution at early times and finally wind up below it at late times. That is, these states decay too fast to remain very long in a Boltzmann distribution.

After the lower vibrational levels ($E_\lambda \lesssim 4000 \ cm^{-1}$) have reached a Boltzmann distribution at an effective temperature $T_{eff}(t_0)$, Eq. (3.5) describes their subsequent relaxation until $T_{eff}(t)$ begins to approach the gas temperature T. At that point n_λ is no longer proportional to $\exp(-\gamma_\lambda t)$; consequently Eq. (3.5) is no longer valid. At these late times $T_{eff}(t)$ asymptotically approaches the gas temperature but it was not possible to experimentally determine its functional dependence on time due to the problems with three-body recombination mentioned earlier. These observations agree with the theoretical results obtained by Montroll and Shuler[10] for the relaxation of a dilute gas of harmonic oscillators in contact with a constant temperature heat bath. They found that an initial Boltzmann distribution at a temperature T_0 relaxes to a final equilibrium Boltzmann distribution at the temperature T of the heat bath via a continuous sequence of Boltzmann distributions described by an effective temperature. At early times their effective temperature has exactly the same time dependence as our Eq. (3.5) and at late times they find an exponential approach to the gas temperature T in qualitative agreement with our observations at late times.

A quantitative comparison can be made with Montroll and Schulers result for the time period when Eq. (3.5) is valid; however, one must first emphasize that (1)

their results are based on a harmonic oscillator model in which transitions are allowed only between adjacent vibrational levels, and (2) this vibrational transition rate is assumed to increase linearly with the vibrational energy [see Eq. (1.1) of Ref. 10]. The Hg_2 potential given in Table II and Fig. 10 of Ref. 3 may be crudely approximated by a harmonic oscillator for the lower vibrational levels and the relaxation rate k_λ plotted in Fig. 9 of the present paper is linear in E_λ; thus the model of Montroll and Shuler may be applicable to our low lying vibrational levels in a semiquantitative fashion. Comparing our Eq. (3.5) with their Eq. (1.12a) we obtain a vibrational transition rate $k_{10} \simeq 5.2 \times 10^{-11} \ cm^3 \ sec^{-1}$ for transitions between the two lowest vibrational levels at a gas temperature of 673 °K. This is slightly larger than the $E_\lambda = 0$ intercept in Fig. 9 but we would expect the vibrational transition rate to be faster than the relaxation rate since the latter is a balance between collisional gain and loss terms.

The model of Montroll and Shuler is not applicable to the higher vibrational levels ($E_\lambda > 400 \ cm^{-1}$) because this region of the potential curve may not be approximated by a harmonic oscillator (see Fig. 10 of Ref. 2) and the vibrational relaxation rate k_λ is not proportional to the vibrational energy.

At this point, one may wonder why we saw no population inversion at the earliest times. That is, the time labeled zero in Figs. 3 and 6 is roughly coincident with the peak of the pump laser pulse yet the population is already thoroughly spread to the lower states rather than being concentrated around the pumped state as one might expect. This is due to the extremely fast vibrational relaxation rates which spread the excitation to lower vibrational levels before the pump laser pulse is terminated. In the Appendix we outline the relaxation of a simple two state system which illustrates this process mathematically. It is interesting to note that the relaxation rates $3 \times 10^{-10} \ cm^3 \ sec^{-1}$ and $5 \times 10^{-11} \ cm^3 \ sec^{-1}$, corresponding to the highest and lowest vibrational levels (see Fig. 9), give collision diameters the order of 5 Å and 2.5 Å, respectively. These values compare favorably with the internuclear separations corresponding to the top and bottom of the 1_u potential curve (see Table II of Ref. 3).

We next consider the temperature dependence of γ_λ plotted in Fig. 5 which shows that the decay rate at the bottom of the 1_u well (e.g., $\lambda = 340$ nm) decreases with increasing temperature, whereas the decay rate for higher vibrational levels (e.g., $\lambda = 260$ nm) increases with temperature. These observations may be explained qualitatively by noting that collisional relaxation of states at the bottom of the 1_u well requires an electronic transition to some of the lower lying states. Since electronic transition rates are usually slower than purely vibrational transitions, the collisional relaxation rate should be somewhat slower at the bottom of the 1_u well as is observed in Fig. 5. Furthermore, the net relaxation rate will be the downward collision rate minus the rate at which the $E_\lambda = 0$ level gains population through vibrational transitions from higher levels and upward transitions from low

lying electronic states. The later process will have an exponential temperature dependence, $\exp(-\Delta E/kT)$, where $\Delta E < 2800$ cm^{-1} (see Table I of Ref. 1) which will cause the net relaxation rate to decrease with increasing temperature as is observed. For higher levels, the collisional loss rate is larger due to downward vibrational transitions and the upward rate from low lying electronic states is smaller due to the increase in ΔE; consequently the temperature dependence of k_λ should become weaker for shorter wavelengths, as is also observed in Fig. 5. Finally, the vibrational level which emits at 260 nm lies about kT below the $6\,^3P_0$ atomic state and may therefore be lost by collisional dissociation, which could explain the increase in k_λ with increasing temperature.

One remaining observation which must be explained is the fact that most of the pump laser energy is converted into $^3P_0$ atoms. Integrating over time and wavelength we find that the intensity spike at early times represents only 10^{-2} or 10^{-3} of the total emission intensity. Since the pump laser pulse at 254.5 nm excites vibrational levels which lie about 1500 cm^{-1} (or 10 vibrational levels)[2,3,6] above the $6\,^3P_0$ state, and since all states are relaxed mainly by collisions (i.e., $nk_\lambda \gg \tau_\lambda^{-1}$ for $n \gtrsim 10^{17}$ cm^{-3}), this would imply that the $1_u \rightarrow 0_u^-$ collision rate is much faster than the vibrational relaxation rate. To explain how this can happen, we recall that the relaxation rate k_λ, defined in Eq. (3.2), is the difference of collisional loss and gain rates. Thus the relaxation rates will generally be smaller than the collision rates R and r. However, for vibrational levels lying above the $6\,^3P_0$ atomic state, a $1_u \rightarrow 0_u^-$ transition results in dissociation of the molecule and the back rate opposing this loss mechanism, namely, three-body molecular formation, is so much smaller it may be ignored. Thus, even though the vibrational transition rates R may be faster than the $1_u \rightarrow 0_u^-$ transition rate, the relaxation of these high lying levels can be dominated by the $1_u \rightarrow 0_u^-$ transitions because the latter are not opposed by a back rate.

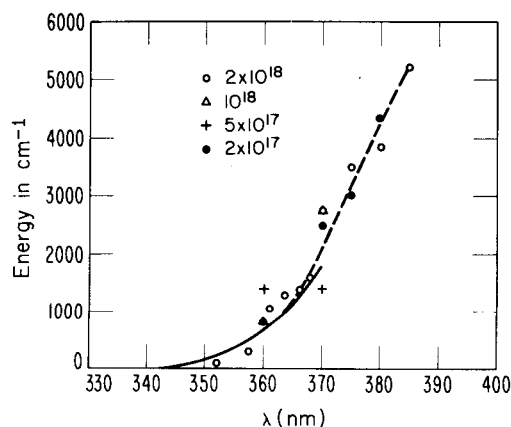If we therefore equate the relaxation rate at 260 nm

FIG. 10. Potential energy curve for the 1_u state as a function of fluorescence wavelength in the red wing of the 335 nm band. Measurements were made at several different densities to illustrate the amount of scatter in the data.

TABLE I. Potential energy curve for the repulsive wall of the Hg$_2$(1_u) state corresponding to the red wing of the 335 nm band. These data extend the potential energy data given in Table II of Ref. 3. Ground state and excited state energies are in cm^{-1}, and the internuclear distance R is given in both atomic units and angstroms (the latter in parentheses).

λ (nm)	R	Ground state	Excited state
340	5.48 (2.90)	2 090	31 502
345	5.40 (2.86)	2 555	31 541
350	5.33 (2.82)	3 088	31 659
355	5.26 (2.78)	3 698	31 867
360	5.19 (2.74)	4 399	32 177
365	5.11 (2.72)	5 210	32 608
370	5.02 (2.65)	6 522	33 550
375	4.93 (2.61)	7 983	34 650
380	4.85 (2.57)	9 434	35 750
385	4.78 (2.53)	10 826	36 800

and 257 nm with the $1_u \rightarrow 0_u^-$ transition rate, we obtain a rate coefficient of 2.7×10^{-10} cm^3 sec^{-1} which compares favorably with the value 1.6×10^{-10} cm^3 sec^{-1} obtained in Ref. 1 for $1_u \rightarrow 0_g^-$ transitions.

IV. EXTENSION OF THE 1$_u$ POTENTIAL ENERGY CURVE

The lack of trimer emission during the first 200 nsec following the pump laser pulse permits us to study the intensity in the red wing of the 335 nm band without interference from the blue wing of the 485 nm band. It is thus possible to extend the previous analysis[3] of the 1_u potential energy curve to smaller internuclear distances. To do this we note that, for a fixed temperature and density, the decay rates increase monotonically with decreasing wavelength (e.g., Fig. 4). That is, each vibrational level has a different decay rate. We may therefore determine the energy E_λ' of the state which emits the wavelength λ' in the red wing by first measuring the decay rate at this wavelength then finding the wavelength λ in the blue wing which has the same decay rate. Since the decay rates are the same, both λ and λ' must be emitted by the same state; hence the unknown E_λ' equals the known value of E_λ (the values of E_λ may be determined from Table II of Ref. 3).

The results of such a calculation are shown in Fig. 10. For some wavelengths, measurements were made at several different densities in order to get some idea as to the uncertainty in the data. The solid curve is the portion of the 1_u potential for the red wing obtained in Ref. 3. The dashed curve represents an extension of the potential energy curve using the data obtained above. The values obtained in Ref. 3 seem slightly low for $\lambda > 365$ nm but this is not too surprising since the edges of the bands were subject to the greatest error in Ref. 3.

The potential curve for $\lambda \gtrsim 340$ nm is tabulated in Table I using the values obtained from Ref. 3 for $340 \le \lambda \le 365$. The internuclear distance R corresponding to each value of λ was obtained, as in Ref. 3, by first calculating the ground state energy (subtract $h\nu_\lambda$ from

the excited state energy) then comparing with the theoretical calculation of Baylis and Walornyi[11] to find the value of R corresponding to that ground state energy.

V. SUMMARY

The decay of the 335 nm Hg_2 fluorescence band has been analyzed at early times where vibrational relaxation in the dimer can be studied without interference from three-body processes which proceed at a much slower rate.

It was found that the vibrational relaxation rate increases exponentially with vibrational energy (Fig. 9). Observation of the photon yield at early and late times indicates that the branching ratio for formation of $6\,^3P_0$ atoms is 10^2–10^3 times larger than direct vibrational relaxation. The relaxation of the highest levels was therefore ascribed to $1_u \rightarrow 0_g^-$ transitions resulting in a rate of 2.7×10^{-10} cm^3 sec^{-1}. The lower vibrational levels ($E_\lambda \le 4000$ cm^{-1}) very quickly formed a Boltzmann distribution at an effective temperature T_{eff}. This effective temperature then decayed with time asymptotically approaching the gas temperature T. The time dependence of $T_{eff}(t)$ at early times [before $T_{eff}(t) \simeq T$] agreed with the model calculations of Montroll and Shuler,[11] who calculated the relaxation of a gas of harmonic oscillators. Since the assumptions of their model seem reasonably well satisfied for the lower vibrational levels in Hg_2, a quantitative comparison was made which gave a vibrational transition rate of 5.2×10^{-11} cm^3 sec^{-1} for the $v = 1$ to $v = 0$ transition. This value is consistent with our measurements of the vibrational relaxation rate shown in Fig. 9.

Since no mercury trimers have been formed at these early times, it was possible to examine the red wing of the 335 nm dimer band without interference from the 485 nm trimer band. This analysis enabled us to calculate part of the repulsive wall of the 1_u potential curve for the dimer. These data are given in Table I.

APPENDIX

In this Appendix we will outline a simple two state model which illustrates the early time behavior of our optically excited vibrational states. We consider the population $n_1(t)$ of the vibrational level which is directly excited by a pump pulse $P(t)$, and the population of a lower vibrational level $n_0(t)$ which is coupled to n_1 by collisions. These populations will be described by the rate equations

$$\dot{n}_1(t) = -\Gamma_1 n_1(t) + \Gamma_{10} n_0(t) + P(t), \qquad (A1)$$

$$\dot{n}_0(t) = -\Gamma_0 N_0(t) + \Gamma_{01} n_1(t), \qquad (A2)$$

where $\Gamma_1 = A + \Gamma_{01}$ and $\Gamma_0 = A + \Gamma_{10}$ (we assume that both states have the same radiative A value denoted simply by A) while Γ_{10} and Γ_{01} denote $0 \rightarrow 1$ and $1 \rightarrow 0$ collision rates, respectively. These equations are easily converted into uncoupled second order equations

$$\ddot{n}_1(t) + (\Gamma_0 + \Gamma_1)\dot{n}_1 + (\Gamma_0\Gamma_1 - \Gamma_{01}\Gamma_{10})n_1 = \Gamma_0 P(t) + \dot{P}(t), \quad (A3)$$

$$\ddot{n}_0(t) + (\Gamma_0 + \Gamma_1)\dot{n}_0 + (\Gamma_0\Gamma_1 - \Gamma_{01}\Gamma_{10})n_0 = \Gamma_{01}P(t), \qquad (A4)$$

with solutions

$$n_1(t) = \int_0^t [\Gamma_0 P(s) + \dot{P}(s)]\, G(t\,|\,s)\, ds, \qquad (A5)$$

$$n_0(t) = \int_0^t \Gamma_{01} P(s)\, G(t\,|\,s)\, ds, \qquad (A6)$$

where

$$G(t\,|\,s) \equiv (e^{-\lambda_s(t-s)} - e^{-\lambda_f(t-s)})/(\gamma_f - \gamma_s), \qquad (A7)$$

$$\left\{ \begin{matrix} \gamma_f \\ \gamma_s \end{matrix} \right\} \equiv \left(\frac{\Gamma_0 + \Gamma_1}{2}\right) \pm \frac{1}{2}\sqrt{(\Gamma_0 + \Gamma_1)^2 - 4(\Gamma_0\Gamma_1 - \Gamma_{01}\Gamma_{10})}$$

$$= \left\{ \begin{matrix} A + \Gamma_{01} + \Gamma_{10} \\ A \end{matrix} \right\}. \qquad (A8)$$

For simplicity we will let $P(s)$ be a square pulse of amplitude p and duration T, then for $t \le T$,

$$n_1(t) = \frac{p\Gamma_0}{(\gamma_f - \gamma_s)}\left[\left(\frac{1 - e^{-\gamma_s t}}{\gamma_s}\right) - \left(\frac{1 - e^{-\gamma_f t}}{\gamma_f}\right)\right]$$
$$+ p\left(\frac{e^{-\gamma_s t} - e^{-\gamma_f t}}{\gamma_f - \gamma_s}\right), \qquad (A9)$$

$$n_0(t) = \frac{p\Gamma_{01}}{\gamma_f - \gamma_s}\left[\left(\frac{1 - e^{-\gamma_f t}}{\gamma_s}\right) - \left(\frac{1 - e^{-\gamma_f t}}{\gamma_f}\right)\right]. \qquad (A10)$$

In our case $T \simeq 10$ nsec, $A \simeq 10^7$ sec^{-1}, $\Gamma_{01} \ge 3 \times 10^{-10} n$ (taking the relaxation rate for the highest vibrational levels from Fig. 9) and $\gamma_{10} \simeq \Gamma_{01}\exp(-\Delta E/kT)$, where the energy spacing of the 0 and 1 states is denoted by ΔE. With these values, $\gamma_s \simeq 10^7$ $sec^{-1} \ll \gamma_f \simeq 3 \times 10^{-10} n$ (for $n \ge 5 \times 10^{17}$ cm^{-3}); thus, for $t \simeq T = 10$ nsec, $\gamma_s T \ll 1$ and $\gamma_f T > 1$ or $\exp(-\gamma_s T) \simeq 1 - \gamma_s T$ and $\exp(-\gamma_f t) \ll 1$. Using these relations, Eqs. (A9) and (A10) give

$$n_1(T) \simeq (\Gamma_0 T + 1)\,(p/\gamma_f), \qquad (A11)$$

$$n_0(T) \simeq \Gamma_{01} T\,(p/\gamma_f). \qquad (A12)$$

Finally, since $\Gamma_{01}T > 1$ and $\Gamma_{01} > \Gamma_0$ we see that $n_0 T > n_1(T)$. That is, the population inversion which exists at very early times $t < 1/\Gamma_{01}$ (due to the fact that we are pumping only the 1 state) is destroyed in a time on the order of our pump laser pulse.

It should be noted that Eq. (A11) is extremely sensitive to the switching transient [$\dot{P}(s)$ term in Eq. (A5) and second term in Eq. (A9)] which results from our choice of a square pulse. For a smoother pulse this effect would be reduced and Eq. (A11) would be closer to $\Gamma_0 T(p/\gamma_i)$ which is much smaller. Secondly the rate $\Gamma_{01} = (3 \times 10^{-11})n$ is probably too small since the vibrational transition rate Γ_{01} is expected to be somewhat larger than the observed relaxation rate. Correcting these two approximations will make the ratio $n_0(T)/n_1(T)$ even larger.

[1]M. Stock, E. W. Smith, R. E. Drullinger, and M. M. Hessel (submitted to J. Chem. Phys).
[2]R. E. Drullinger, M. M. Hessel, and E. W. Smith, J. Chem. Phys. 66, 5656 (1977).
[3]E. W. Smith, R. E. Drullinger, M. M. Hessel, and J. Cooper, J. Chem. Phys. 66, 5667 (1977).
[4]D. J. Eckstrom, R. A. Gutcheck, R. M. Hill, D. Heustis,

and D. C. Lorents "Studies of E-beam pumped molecular lasers," Stanford Research Institute Tech. Rep. MP 73-1, July 31, 1973.

[5]P. J. Hay and R. C. Raffenetti, J. Chem. Phys. 65, 2679 (1976); F. Mies, M. Krauss, and W. J. Stevens (manuscript in preparation).

[6]M. Stock, E. W. Smith, R. E. Drullinger, and M. M. Hessel (submitted to J. Chem. Phys.).

[7]H. Takeyama, J. Sci. Hiroshima Univ. 15, 235 (1952).

[8]G. Herzberg *Molecular Structure and Molecular Structure 1. Spectra of Diatomic Molecules* (Van Nostrand Reinhold, New York, 1950), 2nd ed.

[9]R. Landenberg and G. Wolfsohn, Z. Phys. 63, 616 (1930); J. P. Barrat, J. Phys. Radium 20, 541, 633, 657 (1959); P. Platz, J. Phys. (Paris) 32, 784 (1971); E. Luc-Koenig, J. Phys. B 7, 1052 (1974); J. N. Dodd, W. J. Sandle, and O. M. Williams, J. Phys. B 3, 256 (1971); Andersen, Jessen, and Sorensen, Nucl. Instrum. Methods 90, 35 (1971).

[10]E. W. Montroll and K. E. Shuler, J. Chem. Phys. 26, 454 (1957). Note that the first θ on the right hand side of Eq. (1.12a) should be θ_0.

[11]W. Baylis and Walornyi (work in progress).